

## Article

# New Concept Ocean-Bottom Multiphysics (OBMP) Nodes for Reservoir Monitoring

Paulo T. L. Menezes <sup>1,2,\*</sup> , Andrea Zerilli <sup>3</sup> , Jorlivan L. Correa <sup>1</sup>, Everton N. Menor <sup>1</sup>, Sergio M. Ferreira <sup>1</sup> and Tiziano Labruzzo <sup>3</sup>

<sup>1</sup> PETROBRAS-EXP/PEN/AB, Av. Henrique Valadares 28, 4 andar, Rio de Janeiro 20231-030, Brazil

<sup>2</sup> Departamento de Geologia Aplicada, Faculdade de Geologia/UERJ, Rua São Francisco Xavier, 524, sala 2009 Bloco A, Rio de Janeiro 20550-900, Brazil

<sup>3</sup> Zlemlink Ltda., Rua Taylor 39 sala 805, Rio de Janeiro 24241-060, Brazil

\* Correspondence: ptarsomenezes@petrobras.com.br or paulo.menezes@uerj.br

**Abstract:** Marine-controlled source electromagnetics (CSEM) have been extensively applied to various exploration scenarios worldwide. However, its perceived value and cost relative to seismic and the scarcity of realistic case studies have limited the industry's interest in time-lapse reservoir-monitoring (4D) applications. A feasible way to make demand for CSEM for 4D-monitoring programs would be to increase the value of information and reduce survey costs by performing joint operations where seismic and CSEM data are acquired during the same survey and at equivalent spatial densities. To this end, we propose a new multiphysics ocean-bottom nodes (OBN) concept and show the industry that CSEM can be a cost efficient and effective integrators to 4D seismic projects. To this end, we conducted a feasibility study demonstrating that horizontal magnetic field components have the required sensitivities and can be used instead of horizontal electric field components in mapping the 3D resistivity distribution and 4D fluid change responses in a given reservoir. This makes engineering a new OBN class simpler and cheaper, as various miniaturized magnetic field sensors are available off-the-shelf or readily working along with packaging and coupling solutions.

**Keywords:** reservoir monitoring; CSEM; ocean-bottom nodes; multiphysics acquisition



**Citation:** Menezes, P.T.L.; Zerilli, A.; Correa, J.L.; Menor, E.N.; Ferreira, S.M.; Labruzzo, T. New Concept Ocean-Bottom Multiphysics (OBMP) Nodes for Reservoir Monitoring. *Minerals* **2023**, *13*, 602. <https://doi.org/10.3390/min13050602>

Academic Editor: Georgy Cherkashov

Received: 10 January 2023

Revised: 26 February 2023

Accepted: 8 March 2023

Published: 27 April 2023



**Copyright:** © 2023 by the authors. Licensee MDPI, Basel, Switzerland. This article is an open access article distributed under the terms and conditions of the Creative Commons Attribution (CC BY) license (<https://creativecommons.org/licenses/by/4.0/>).

## 1. Introduction

During the last  $20 \pm$  years, marine CSEM has been applied for de-risking deep-water high-cost drilling decisions in many basins worldwide. From the early days, CSEM has been expanded to a broader range of geographic areas, geological environments, and application scenarios. Ongoing development efforts have demonstrated the potential to enhance cost-effective deep-water reservoir-monitoring applications. Indeed, several pioneering feasibility studies (e.g., [1–3]) have revealed that time-lapse (4D) CSEM can play a role in improving our knowledge of the reservoir structure, fluid flow, and fluid saturation changes when appropriate acquisition and advanced integrated interpretation workflows are applied.

Nonetheless, a single 4D CSEM survey has been reported in the literature [4]. We attribute the perceived value and cost of CSEM, relative to seismic acquisition, to the lack of realistic case studies, and, most of all, the lack of new developments and investments in effective 4D acquisition systems as the main reasons the industry has not yet considered CSEM in 4D reservoir-monitoring programs.

CSEM uses a horizontal electric dipole source towed along a line by a surface vessel, usually as close to the seafloor as possible (commonly 30–50 m). The source transmits an EM signal through the seafloor at user-defined frequencies, usually in the 0.1–10 Hz range. The ocean-bottom electromagnetic (OBEM) receivers, which measure the horizontal electric and/or magnetic fields, are placed on the seafloor either in a free-fall operation along a

line (for 2D) or grid (for 3D) pattern, with typical OBEM spacing in the 1–3 km range for hydrocarbon exploration purposes (Figure 1).

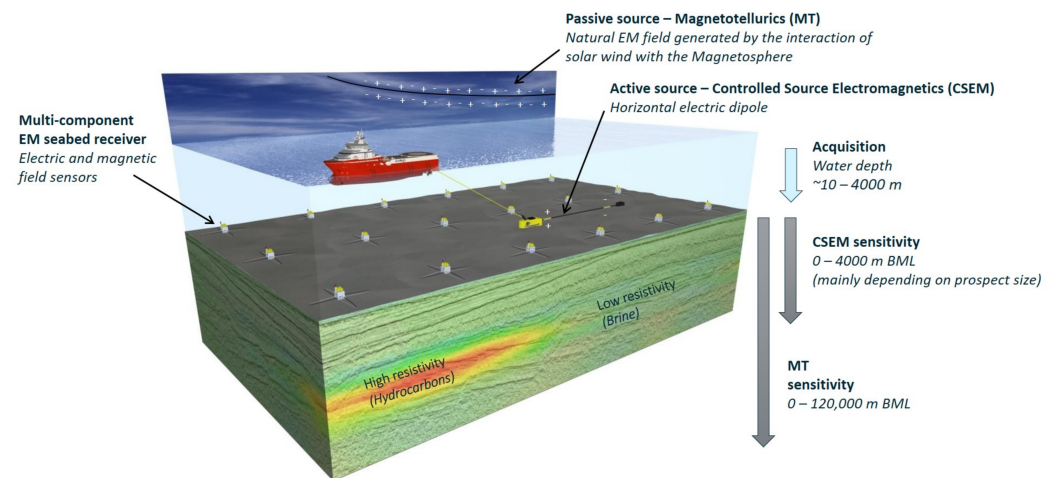


**Figure 1.** Acquisition scheme and sensitivity below mud line (BLM) of MT and CSEM methods. Courtesy of EMGS.

The current industry’s state-of-the-art CSEM nodes are equipped with electric field dipoles of 8 to 10 m and two to three induction coils for the magnetic field measurements [5,6]. The nodes are attached to 200 kg concrete anchors, used to sink the instruments from the surface to the ocean bottom. Present-day CSEM ships can store hundreds of receivers [7]. Surveying large areas and/or denser receiver spacings often affects the efficiency and, consequently, the costs of a given project.

Dedicated 4D ocean-bottom node (OBN) surveys comprise most of the current time-lapse seismic projects. Acquisitions are designed to maximize position repeatability, and timing is planned to impact reservoir management. The OBN surveys have seen exponential progress in cost efficiency, with the cost per trace reducing by approximately 50% every two years [8]. Ultra-compact sensors (1 m) drastically increase node count onboard (1000–10,000 nodes), enabling far denser sampling and significantly improving ROV (remotely operated vehicles) operational efficiency (Figure 2).

A possible way to step up CSEM into a cost-efficient integrator to a 4D seismic program might be to conduct multiphysics surveys, where seismic and CSEM data are jointly acquired during the same survey, comparable to marine gravity and magnetic-seismic joint acquisitions. Going back to basics, reassessing every aspect of CSEM, from node redesign and deployment to operational efficiency, is required to show the industry that CSEM could be a cost-efficient and effective integrator.

According to [7], one of the keys to success is the development of seismic-EM bundled-integrated ocean-bottom multiphysics (OBMP) nodes inspired by and following the current seismic OBN industry searching for better data, efficiency, cost, and simplicity. Ultra-compact nodes facilitate far denser sampling and greatly enhanced operational efficiency, which demands optimization, higher sensitivities, and miniaturization of the EM sensors to integrate them within the current state-of-the-art seismic nodal technology. This may be the case to acquire the magnetic field only, neglecting the electric field, as the magnetic sensors could be easier and faster to incorporate into an ultra-compact node.

A potential issue with our proposition is that CSEM quantitative interpretations are, presently, performed solely with the horizontal electric field components. The magnetic field components recorded in the OBEM nodes are used mainly to compute magnetotelluric responses. Nevertheless, few published studies show that the magnetic field has comparable sensitivity to the electric field in the CSEM interpretation.

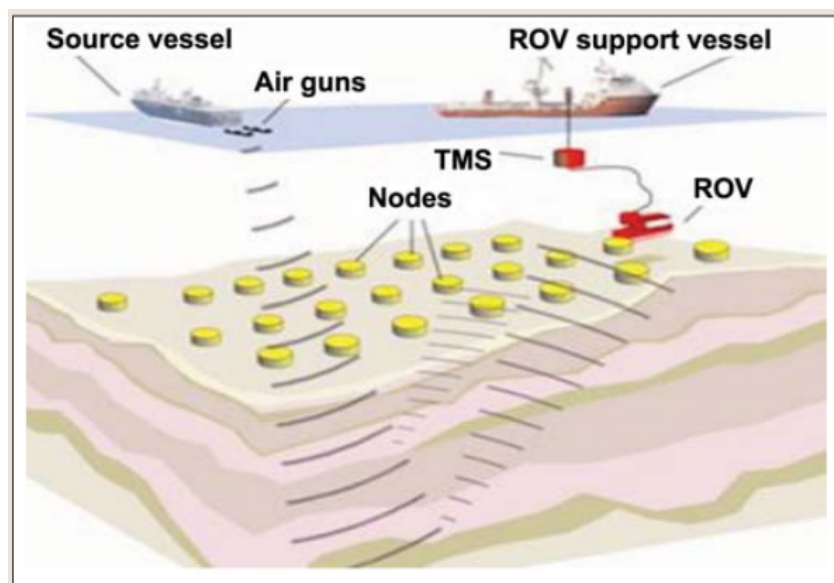


**Figure 2.** Seismic OBN concept. The tether management system (TMS) separates the ROV (remotely operated vehicles) from the vessel heave and the surface umbilical mass, which allows the ROV more freedom of movement. Modified from [9].

Using a synthetic canonical 1D reservoir model, Key (2009) [10] showed that separate 1D inversions of the electric and magnetic fields perform equally well at recovering the reservoir. Key (2009) [10] also concluded that recording only a single field type would be adequate for specific exploration applications.

Constable et al. (2019) [11] interpreted a CSEM dataset acquired at the Scarborough gas field, Australia. They carried out 2D inversions of various data combinations to define how well they recovered the expected reservoir's properties and shape. As a result, they showed that individual inversions of the electric and magnetic components generate almost identical models, suggesting that these datasets do not carry independent information.

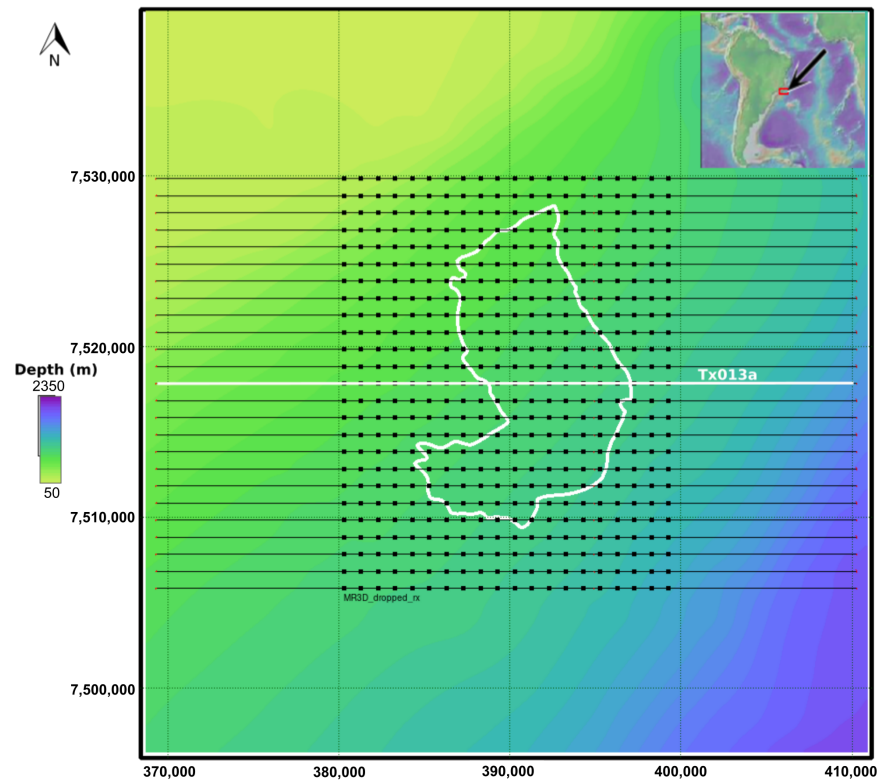
3D inversions of CSEM data were conducted by Tharimela et al. (2019) [12] to investigate gas hydrate accumulations in the Pelotas Basin, Brazil. They showed that the magnetic field inversions provided smoother models that were more compatible with seismic events when compared with electric field inversions. These results were further confirmed by synthetic modelling and inversion studies using simple theoretical models. They attributed the spurious anomalies of the electric inversions to the static shift phenomena that affect the electric field only.

Herein we develop the findings of [13] and demonstrate that the horizontal magnetic field components ( $H_x$ ,  $H_y$ ) can be effectively used for 3D appraisal studies and 4D-monitoring applications. We conducted a time-lapse feasibility study based on the MR3D realistic turbiditic model [14] employing the horizontal magnetic components of the 4D CSEM dataset calculated by [3]. We show that the horizontal magnetic field inversion outcomes are comparable to the horizontal electric field inversions and are sensitive to map time-lapse resistivity changes associated with oil–water substitution in the studied reservoir.

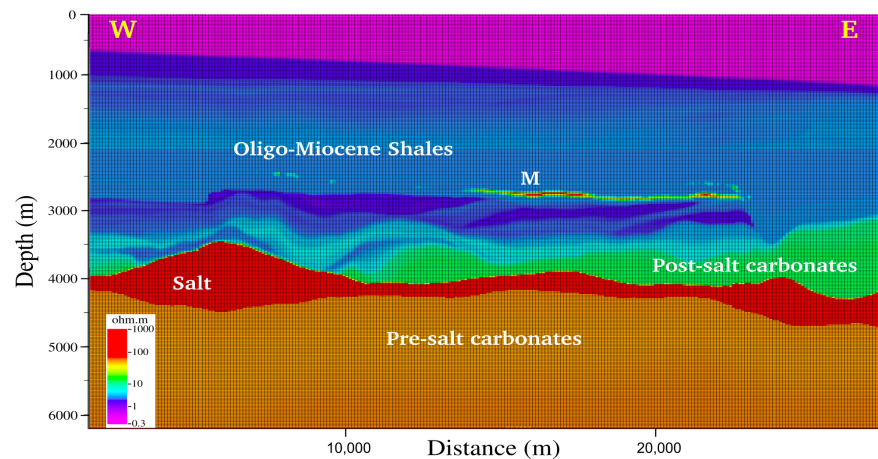
## 2. MR3D Project

Marlim R3D (MR3D) is an open-source project aiming to supply a realistic geoelectric model to be employed as a benchmark for CSEM studies of the Brazilian continental margin deep-water turbidites reservoir systems. These turbidites are considered analogues to several others worldwide, such as those found in the African continental margin. Recently, refs. [14,15] made the MR3D geoelectric model and the synthetic-associated CSEM dataset public, respectively.

The MR3D VTI model was constructed based on the geological knowledge of the mature Marlim oilfield [16], located in the northeastern portion of the offshore Campos Basin, Brazil (Figure 3a). Marlim is a heavy oil field discovered in 1985 at water depths ranging from 600 to 1200 m (Figure 3a). Oil production began in 1991 and seawater injection also started by that year [17].



(a)



(b)

**Figure 3.** (a) Marlim field with the CSEM acquisition geometry superimposed on bathymetry. The reservoir outline is displayed as a white line. Black dots show the receiver locations distributed in a 1000 m spacing regular grid. Black lines are source west–east towlines evenly spaced at 1000 m. Towline Tx013a is highlighted as the white line. (b) Cross-sections of the MR3D model along the east–west towline Tx013a. Marlim oil-prone turbidites (M) appear as the thin resistive body embedded in the Oligocene–Miocene shales sequence. Modified from [13].

The MR3D model mixes fine-scale stratigraphy and complex oil-filled reservoirs in a complex geological environment consisting of Oligocene–Miocene shales, post-salt carbonates, a thick Aptian salt layer, and pre-salt carbonates (Figure 3b). The reservoir facies are formed by high porosity, in the 26–32% range, and clean sandstones [16]. The reservoir has a variable thickness of up to 125 m, with an average of 80 m [17].

The heavy oil reservoirs of the Marlim field are composed of an Oligocene–Miocene deepwater turbidite system of the Carapebus Formation (Figure 4). They include a set of amalgamated sandstone bodies recognized as Marlim sandstone [18]. The turbiditic sedimentation that has occurred was influenced by a regional northwest–southeast trending transfer faults system [19]. This system built the pathway for the deposition, reworking, and displacement of many deepwater turbiditic reservoirs in the Campos Basin [20].

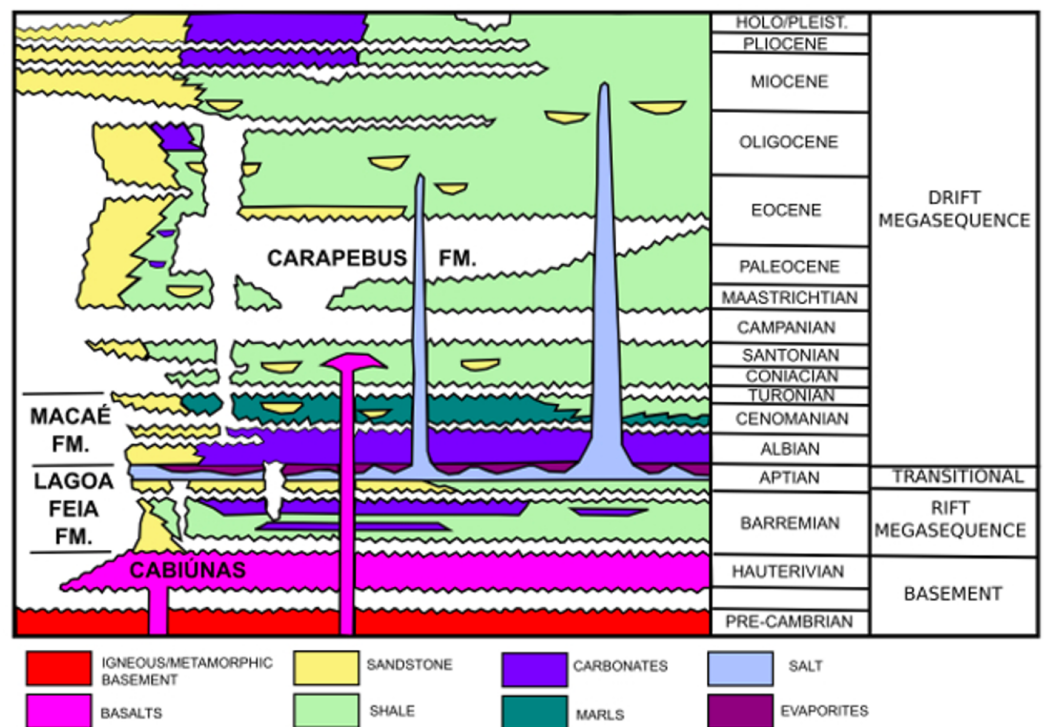
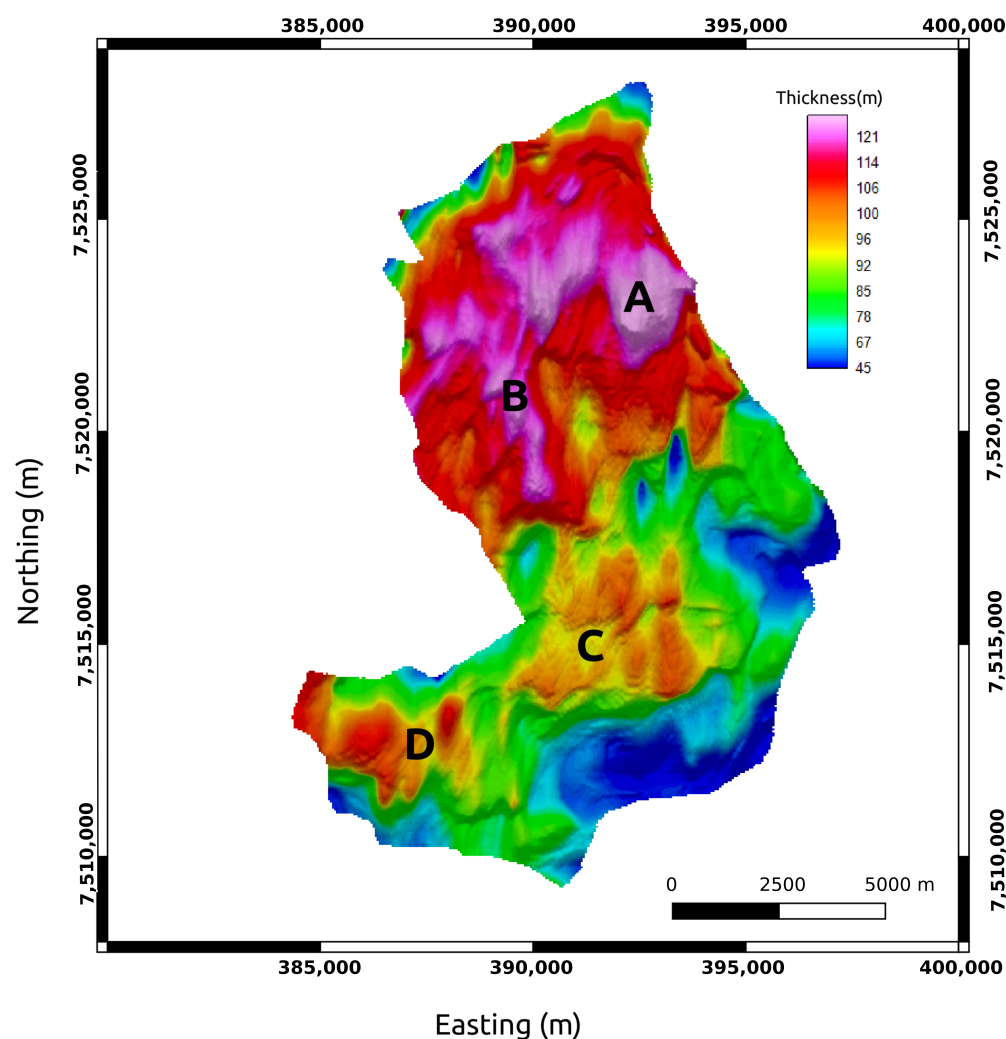


Figure 4. Campos Basin simplified stratigraphic chart, modified from [21].

Figure 5 exhibits the isopach map of the MR3D reservoir with four major thick northwest–southeast trending turbidite lobes (A–D in Figure 5) that comprise the main oil-producing zones of the Marlim field [22].



**Figure 5.** Isopach map of the MR3D reservoir. A–D are thick turbidite lobes and the main oil-producing zones.

### 3. 4D Feasibility

#### 3.1. Forward Modelling—MR4D Data

Menezes et al. (2021) [3] conducted a 4D feasibility study to assess the CSEM effectiveness in detecting resistivity changes associated with water saturation changes within the Marlim reservoir. The starting point of that study was the pre-production scenario (1991) of the MR3D model (Figure 3b). Then, a fluid flow simulator was used to simulate the oil–water substitution for the 2021 and 2031 production years representing 30 and 40 years of production, and seawater injection to build subsurface cellular resistivity models and perform a forward-modelling study.

The flow simulator yielded saturation variations that were then converted into resistivity. The reservoir connection, the relative scarcity of gas, the relative permeability curves, and the field location led to a seawater injection of 600,000 barrels/day as the most viable method for pressure maintenance and oil recovery [17].

In the present study, we extend the findings of [3] by investigating the ability of the magnetic fields to image a 3D oil-filled reservoir and detect time-lapse changes due to fluid replacement within that reservoir. We assume that the resistivity changes are only associated with the fluid substitution within the reservoir's boundaries (Figure 3a), while the background resistivity remains unchanged. Other superficial effects are not considered as they have been thoroughly investigated by [2].

Figure 3a shows the design of the synthetic CSEM survey in MR3D. The survey consists of 25 E–W 1 km spaced towlines and a dense 1 × 1 km grid of 500 OBEM receivers. A 3D forward modelling parallelized commercial fast finite-difference time-domain (FDTD) CSEM modelling algorithm [23] was used to compute all six electromagnetic field components  $E_x$ ,  $E_y$ ,  $E_z$ ,  $H_x$ ,  $H_y$ , and  $H_z$  for six source frequencies of 0.125, 0.25, 0.5, 0.75, 1, and 1.25 Hz.

The noise-free data’s electromagnetic fields were computed with 0.1 s time steps, at a maximum number of 200,000 time steps, and a convergence accuracy of  $10^{-4}$ . The electric fields were normalized by the dipole moment. Multiplicative noise was added with a 1% standard deviation following the procedure of [24]. A noise floor of  $10^{-15}$  V/Am<sup>2</sup> for the electric fields, and  $10^{-12}$  m<sup>-2</sup> for the magnetic fields was applied.

We modelled a horizontal electric dipole source towed 30 m above the seabed. The transmitter current was directed along the towing direction with inline and broadside data registered up to 12 km offsets [14].

The synthetic CSEM data were generated for the 2021 and 2031 monitoring years described above. The modelling exercise delivered high-quality magnetic data to a source-receiver offset up to 12 km for the lower frequencies and maximum ranges of 5 to 6 km for the higher frequencies (Figure 6).

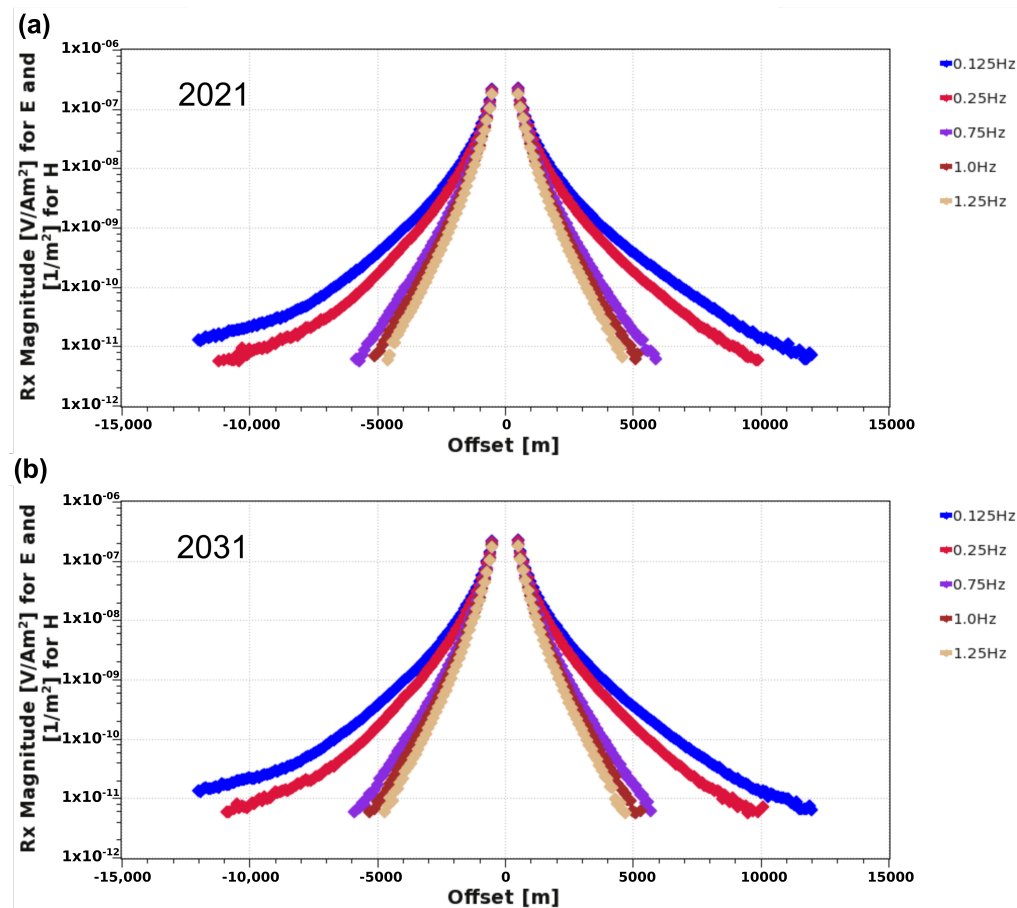


Figure 6. Typical data for the MR3D model showing the inline magnetic field. Site 04Rx251a. (a) 2021 base survey; (b) 2031 monitoring survey.

### 3.2. Inversions for 3D Appraisal and 4D Responses

We then conducted unconstrained 3D quasi-Newton BFGS anisotropic inversions [25] of the horizontal magnetic data ( $H_x$ - $H_y$ ) for the 2021 and 2031 datasets. To compare with the electric data ( $E_x$ - $E_y$ ) inversions results [3], we duplicated the inversion parametrization for both cases: the L1 smoothness norm utilized for the logarithm of the resistivity values, a

mesh of approximately 9 million cells (see Table 1), and the identical starting model, based on previous seismic-EM integrated interpretations [3]. The inversions converged in less than 50 iterations to a satisfactory RMS target misfit of 1.

Figure 7 displays the comparison between the recovered  $R_v$  final model of the base year's (2021) unconstrained anisotropic inversion for the horizontal electric fields (Figure 7a) and the horizontal magnetic fields (Figure 7b). The Ex-Ey and Hx-Hy models were similar, demonstrating that these datasets do not carry independent information [11].

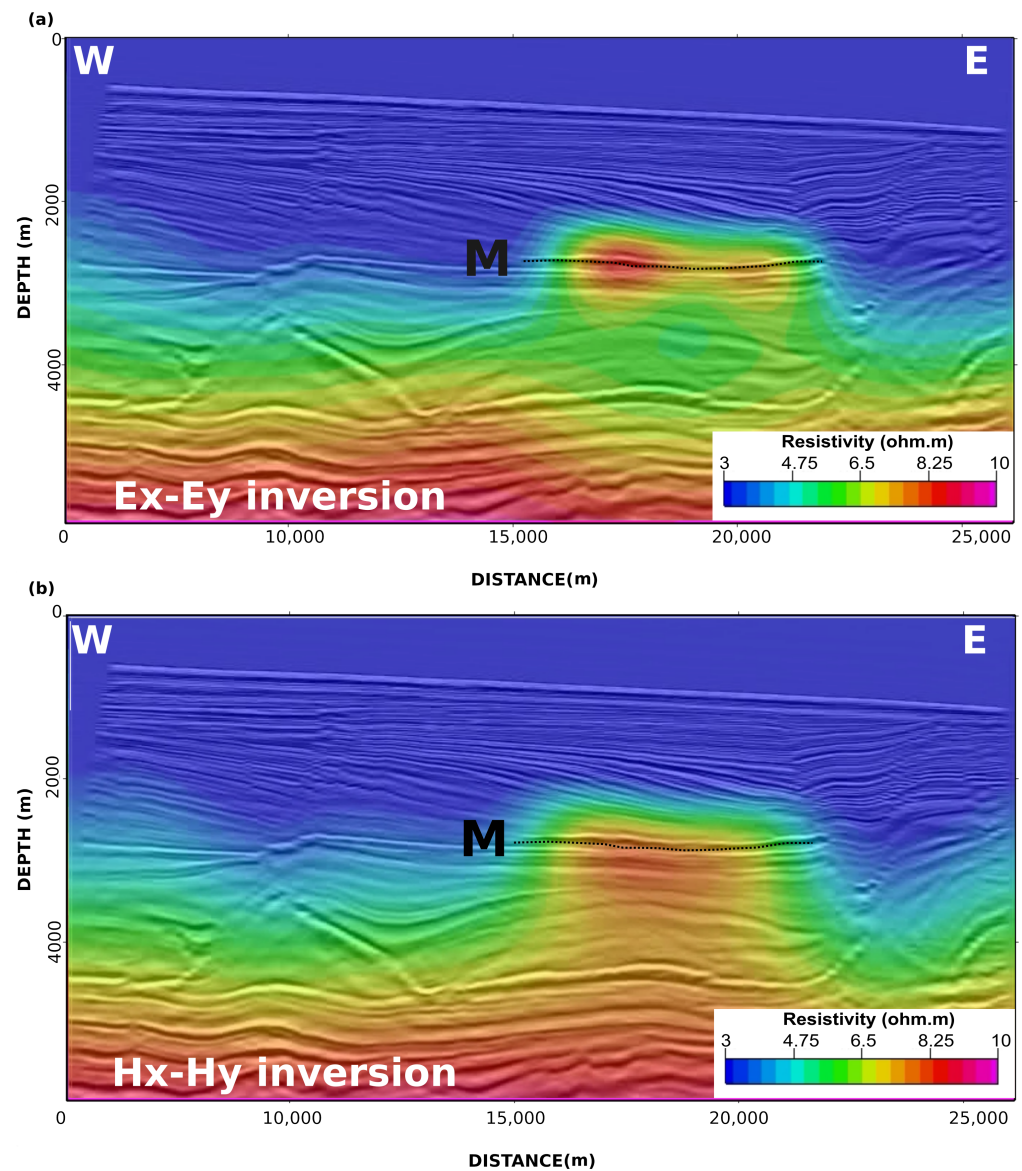


**Figure 7.** Cross-section along line Tx013a (location in Figure 3a—vertical resistivity  $R_v$  for 2021 base year inversions). (a) Horizontal electric fields. (b) Horizontal magnetic fields. Black dotted line defines the lateral extension of the MR3D reservoir (M).

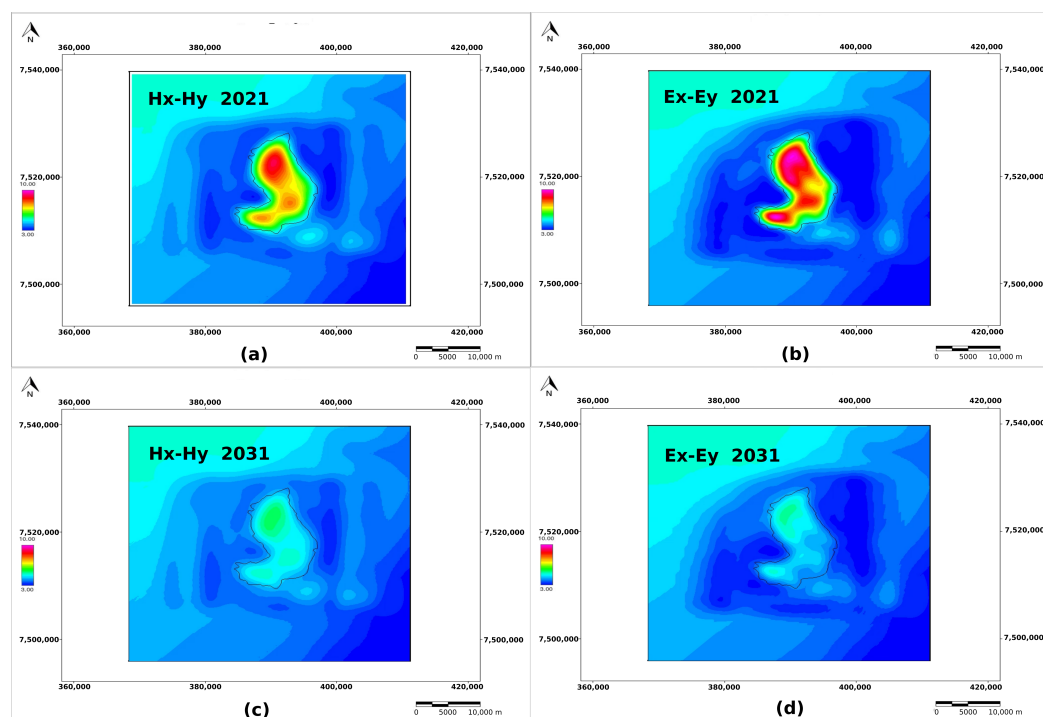
Both extracted cross-sections along the Tx013a line display smooth  $R_v$  anomalies with low vertical resolution around the thin MR3D turbidite horizon at 2650 m depth (M in Figure 7). The resistivity anomalies are reasonably isolated from the resistive background below 3800 m depth. This deep resistor is associated with the deep carbonates and autochthonous salt layers (Figure 3b).

**Table 1.** Mesh used in the MR3D time-lapse BFG inversions.

Mesh Parameters	Dimensions
Cell size - X	200 m
Cell size - Y	200 m
Cell size - Z	50 m
Number of cells - X	220
Number of cells - Y	195
Number of cells - Z	110
Total number of cells	8,910,000.00

Conversely, the horizontal resolution provided by the CSEM method is much higher than the vertical resolution. Consequently, the correlation of anomalies with the associated resistive oil reservoirs is much better imaged when performed along constant depth slices or stratigraphic horizons [26].

Herein we followed the [3] guideline to interpreting the EM attributes extracted within the Marlim reservoir depth interval. We estimated the RMS attribute ( $Rv_{RMS}$ ) of the retrieved  $Rv$  in the  $[-50, +250\text{ m}]$  window around the top of the 2650 m depth slice (Figure 8). As expected, the computed  $Rv_{RMS}$  for the 2021 base year shows an increased horizontal resolution compared to the vertical resolution (Figure 7). The resistive anomalies are fully enclosed within the reservoir's boundaries, and the anomaly borders match the MR3D reservoir outline. Furthermore, one can observe that the magnetic field inversions respond similarly to the electric field inversions, and both respond nicely to the four main producing zones of the MR3D reservoir (Figure 5).

**Figure 8.**  $Rv_{RMS}$  attribute computed at 2650 m depth slice. (a) 2021 Hx-Hy inversion. (b) 2021 Ex-Ey inversion. (c) 2031 Hx-Hy. (d) 2031 Ex-Ey inversion.

We extracted the  $Rv_{RMS}$  attributes for the 2031 inversions at the top of the 2650 m depth slice to demonstrate the time-lapse effect on the CSEM data. Figure 8c shows the  $Rv_{RMS}$  attribute for the Hx-Hy inversion, and Figure 8d the  $Rv_{RMS}$  outcome for the Ex-Ey inversion. Both 2031 inversions also yielded similar models showing a resistive anomaly confined within the MR3D reservoir's boundaries.

By comparing the 2021 base year with the 2031 monitoring year results, we observe a reduction in resistivity anomalies that is in agreement with the flow simulator results of [3], which showed drops in the reservoir's resistivity associated with the fluid substitution for up to 40 years of seawater injection.

These results demonstrate that horizontal magnetic field components can also be effectively used for long-term 4D studies. For the 2031 example (Figure 8c), the stronger anomalies are correlated with the main thickness oil zones within the MR3D reservoir (Figure 5). Indeed, the recovered magnetic anomalies (Figure 8c) are up to 15% stronger than their electric correspondent (Figure 8d).

#### 4. Discussion

Dedicated seismic OBN node surveys make up most of the oil industry expenditure for ongoing and future reservoir-monitoring programs. Although this study claims that the case for CSEM as a promising integrator to 4D seismic is strong, the perceived value and cost needed for additional CSEM measurements inhibit these additional acquisitions in monitoring projects.

Going back to basics, reassessing every aspect of CSEM, from instrument layout and deployment to operational efficiency, is required to demonstrate to the industry that CSEM can be the cost-efficient integrator to 4D seismic as the monitoring requirements become more challenging owing to the high drilling and intervention costs of deep-water reservoir exploration.

This change should begin from the operational side, where most of the cost and efficiency issues reside, by bringing a re-engineered integrated OBMP seabed node (seismic-EM bundled), enabling a single deployment/positioning/recovery cycle and comparable data density inspired and following the current ocean-bottom seismic industry strive for better data, efficiency, cost, and simplicity. The CSEM data would significantly reduce total project costs in such joint seismic-EM investments since the highest expenditures for 4D-monitoring programs are associated with operations and logistics.

#### 5. Conclusions

The Marlim case study reveals that magnetic fields have equivalent sensitivity to that of electric fields to map the 3D resistivity distribution and 4D responses efficiently. Resistivity models in agreement with those estimated from fluid simulators applied to the years 2021 and 2031 were retrieved, thus portraying time intervals of 30 and 40 years, respectively, referring to the pre-production/pre-injection year of 1991.

The use of magnetic sensors could only make re-engineering nodes simpler and cheaper. Various miniaturized magnetic field sensors, along with more straightforward packaging and coupling solutions, are available off-the-shelf or readily operational.

When the global deep-water oil industry is set to emerge stronger and prepared for the subsequent phase of improvements, the time could be suited for an industry-funded OBMP reservoir-monitoring system that will add substantial value to reservoir surveillance decisions guiding more efficient recovery, diminished costs, and raised valuable information. Our feasibility study is encouraging as we envision the needs, potential, and challenges when we come together with the seismic industry and might further persuade us to feel securer about our return on investments.

**Author Contributions:** Conceptualization, P.T.L.M. and A.Z.; methodology, P.T.L.M., J.L.C. and A.Z.; validation, P.T.L.M., J.L.C. and E.N.M.; writing—original draft preparation, P.T.L.M.; writing—review and editing, P.T.L.M., A.Z., S.M.F., T.L. and E.N.M.; supervision, S.M.F.; project administration, S.M.F. All authors have read and agreed to the published version of the manuscript.

**Funding:** This research was funded by Petrobras.

**Data Availability Statement:** Data associated with this research are confidential and cannot be released.

**Acknowledgments:** We are thankful to the management of Petrobras for the support and permission to publish this work.

**Conflicts of Interest:** The authors declare no conflict of interest. The funders had no role in the design of the study.

### Abbreviations

The following abbreviations are used in this manuscript:

CSEM	Controlled-source electromagnetic
BML	Below mud line
EM	Electromagnetic
OBEM	Ocean-bottom electromagnetic
OBMP	Ocean-bottom multiphysics
VTI	Vertical transverse isotropy
RAR	Resistivity anisotropy ratio
Rv	Vertical resistivity
Rh	Horizontal resistivity
ATR	Anomalous transverse resistance
OWC	Oil–water contact
BFGS	Broyden–Fletcher–Goldfarb–Shannon
RMS	Root-mean-square

### References

- Black, N.; Wilson, G.A.; Gribenko, A.V.; Zhdanov, M.S.; Morris, E. 3D inversion of time-lapse CSEM data based on dynamic reservoir simulations of the Harding field, North Sea. In *SEG Technical Program Expanded Abstracts 2011*; Society of Exploration Geophysicists: San Antonio, TX, USA, 2011; pp. 666–670.
- Shantsev, D.V.; Nerland, E.A.; Gelius, L.J. Time-lapse CSEM: How important is survey repeatability? *Geophys. J. Int.* **2020**, *223*, 2133–2147. [[CrossRef](#)]
- Menezes, P.T.; Correa, J.L.; Alvim, L.M.; Viana, A.R.; Sansonowski, R.C. Time-Lapse CSEM Monitoring: Correlating the Anomalous Transverse Resistance with SoPhiH Maps. *Energies* **2021**, *14*, 7159. [[CrossRef](#)]
- Ziolkowski, A.; Parr, R.; Wright, D.; Nockles, V.; Limond, C.; Morris, E.; Linfoot, J. Multi-transient electromagnetic repeatability experiment over the North Sea Harding field. *Geophys. Prospect.* **2010**, *58*, 1159–1176. [[CrossRef](#)]
- Dong, Z.; Zhang, J.; Yang, G.; Cai, Z.; Lu, Y.; Chen, K. Micro-ocean-bottom electromagnetic receiver for controlled-source electromagnetic and magnetotelluric data acquisition. *Rev. Sci. Instrum.* **2021**, *92*, 044705. [[CrossRef](#)] [[PubMed](#)]
- Constable, S. Instrumentation for marine magnetotelluric and controlled source electromagnetic sounding. *Geophys. Prospect.* **2013**, *61*, 505–532. [[CrossRef](#)]
- Zerilli, A.; Menezes, P.T.L.; Crepaldi, J.L.; Correa, J.L.; Viana, A.R. Ocean-bottom multiphysics—Path to superior reservoir monitoring. In *Proceedings of the SEG/AAPG/SEPM First International Meeting for Applied Geoscience & Energy*; OnePetro: Houston, TX, USA, 2021. [[CrossRef](#)]
- Bunting, T. The Evolution of the OBN Acquisition Solution. In *Proceedings of the EAGE Seabed Seismic Today: From Acquisition to Application*; European Association of Geoscientists & Engineers: Kosterijland, The Netherlands, 2020; Volume 2020, pp. 1–4.
- Walker\*, C.; McIntosh, S. Autonomous Nodes—The Future of Marine Seismic Data Acquisition? In *Proceedings of the 12th International Congress of the Brazilian Geophysical Society & EXPOGEF*, Rio de Janeiro, Brazil, 15–18 August 2011; Society of Exploration Geophysicists and Brazilian Geophysical Society: Riode de Janeiro, RJ, Brazil, 2011; pp. 1–6.
- Key, K. 1D inversion of multicomponent, multifrequency marine CSEM data: Methodology and synthetic studies for resolving thin resistive layers. *Geophysics* **2009**, *74*, F9–F20. [[CrossRef](#)]
- Constable, S.; Orange, A.; Myer, D. Marine controlled-source electromagnetic of the Scarborough gas field—Part 3: Multicomponent 2D magnetotelluric/controlled-source electromagnetic inversions. *Geophysics* **2019**, *84*, B387–B401. [[CrossRef](#)]
- Tharimela, R.; Augustin, A.; Ketzer, M.; Cupertino, J.; Miller, D.; Viana, A.; Senger, K. 3D controlled-source electromagnetic imaging of gas hydrates: Insights from the Pelotas Basin offshore Brazil. *Interpretation* **2019**, *7*, SH111–SH131. [[CrossRef](#)]
- Menezes, P.T.L.; Correa, J.L.; Menor, E.N.; Ferreira, S.M.; Zerilli, A.; Labruzzo, T. Ocean-bottom multiphysics for reservoir monitoring—Increasing the value of information. In *Proceedings of the Second International Meeting for Applied Geoscience & Energy*, Houston, TX, USA, 28 August–1 September 2022; pp. 692–696. [[CrossRef](#)]
- Correa, J.L.; Menezes, P.T. Marlim R3D: A realistic model for controlled-source electromagnetic simulations—Phase 2: The controlled-source electromagnetic data set. *Geophysics* **2019**, *84*, E293–E299. [[CrossRef](#)]
- Carvalho, B.R.; Menezes, P.T.L. Marlim R3D: A realistic model for CSEM simulations-phase I: Model building. *Braz. J. Geol.* **2017**, *47*, 633–644. [[CrossRef](#)]

16. Nascimento, T.M.; Menezes, P.T.; Braga, I.L. High-resolution acoustic impedance inversion to characterize turbidites at Marlim Field, Campos Basin, Brazil. *Interpretation* **2014**, *2*, T143–T153. [[CrossRef](#)]
17. Shecaira, F.S.; Daher, J.S.; Gomes, A.C.A.; Capeleiro Pinto, A.C.; Filoco, P.R.; Gomes, J.A.T.; Freitas, L.C.S.; Balthar, S. Injeção de Água no Campo de Marlim—Uma Abordagem Integrada para o Gerenciamento de Reservatórios. In *Proceedings of the Rio Oil & Gas Expo and Conference*; Brazilian Petroleum Institute—IBP: Rio de Janeiro, RJ, Brazil, 2000; pp. 1–9.
18. Peres, W.E. Shelf-fed turbidite system model and its application to the Oligocene deposits of the Campos Basin, Brazil. *AAPG Bull.* **1993**, *77*, 81–101.
19. Lourenço, J.; Menezes, P.T.L.; Barbosa, V.C.F. Connecting onshore-offshore Campos Basin structures: Interpretation of high-resolution airborne magnetic data. *Interpretation* **2014**, *2*, SJ35–SJ45. [[CrossRef](#)]
20. Cobbold, P.R.; Meisling, K.E.; Mount, V.S. Reactivation of an obliquely rifted margin, Campos and Santos basins, southeastern Brazil. *AAPG Bull.* **2001**, *85*, 1925–1944. [[CrossRef](#)]
21. Guardado, L.R.; Spadini, A.R.; Brandão, J.S.L.; Mello, M.R. Petroleum System of the Campos Basin, Brazil. In *Petroleum systems of South Atlantic margins: AAPG Memoir 73*; Mello, M.R., Katz, B.J., Eds.; AAPG: Tulsa, OK, USA, 2000; Chapter 22, pp. 317–324.
22. Mutti, E.; Cunha, R.S.; Bulhoes, E.; Arienti, L.M.; Viana, A.R. Contourites and turbidites of the Brazilian marginal basins. In *Proceedings of the AAPG Annual Convention & Exhibition*, Houston, TX, USA, 6–9 April 2014.
23. Maaø, F.A. Fast finite-difference time-domain modeling for marine-subsurface electromagnetic problems. *Geophysics* **2007**, *72*, A19–A23. [[CrossRef](#)]
24. Mittet, R.; Morten, J.P. Detection and imaging sensitivity of the marine CSEM method. *Geophysics* **2012**, *77*, E411–E425. [[CrossRef](#)]
25. Zach, J.; Bjørke, A.; Støren, T.; Maaø, F. 3D inversion of marine CSEM data using a fast finite-difference time-domain forward code and approximate Hessian-based optimization. In *SEG Technical Program Expanded Abstracts 2008*; Society of Exploration Geophysicists: Las Vegas, NV, USA, 2008; pp. 614–618.
26. Lyrio, J.C.S.O.; Menezes, P.T.L.; Correa, J.L.; Viana, A.R. Multiphysics anomaly map: A new data fusion workflow for geophysical interpretation. *Interpretation* **2020**, *8*, B35–B43. [[CrossRef](#)]

**Disclaimer/Publisher’s Note:** The statements, opinions and data contained in all publications are solely those of the individual author(s) and contributor(s) and not of MDPI and/or the editor(s). MDPI and/or the editor(s) disclaim responsibility for any injury to people or property resulting from any ideas, methods, instructions or products referred to in the content.